THE JOURNAL OF PHYSICAL CHEMISTRY C
A JOURNAL OF THE AMERICAN CHEMICAL SOCIETY

pubs.acs.org/JPCC

Article

# Engineering the Electronic and Thermal Properties of Two-Dimensional Covalent Organic Frameworks

Muhammad A. Rahman, Sandip Thakur, Patrick E. Hopkins, and Ashutosh Giri*

Cite This: J. Phys. Chem. C 2023, 127, 11157−11166

Read Online

ACCESS | Metrics & More | Article Recommendations | Supporting Information



**ABSTRACT:** Two-dimensional covalent organic frameworks (2D COFs) are a class of modular polymeric crystals with high porosities and large surface areas. Their tunable microstructure (with a wide array of choices for the molecular building block) provides the opportunity for their bottom-up design and potentially tailorable physical properties. In this work, through combined density functional theory (DFT) calculations and molecular dynamics (MD) simulations, we study the influence of different molecular functional groups and varying porosities on the electronic and thermal properties of 2D COFs. More specifically, by performing DFT calculations on 24 different 2D COFs, we demonstrate that one of the main descriptors dictating their band gaps are their mass densities or network porosities. Furthermore, we also find that specific functional groups forming the nodes can lead to larger localization of charge densities resulting in wider band gaps. By performing MD simulations to investigate their thermal properties, we show that (similar to their electronic properties) mass density is also one of the main factors dictating heat conduction, where higher densities are associated with relatively higher thermal conductivities along the 2D sheets. Our spectral energy density calculations provide insights into the highly anharmonic nature of these materials. We find that increasing porosities lead to larger anharmonic interactions and thus reduced thermal conductivities in these materials. Similar to their electronic band gaps, the nodes forming the 2D COFs also have a significant contribution in dictating their thermal conductivities with bigger nodes (accompanied by higher densities) generally resulting in relatively higher thermal conductivities in 2D COFs. Taken together, the resulting changes in the electronic and thermal properties from variations in the building blocks in 2D COFs lend insights into fundamental changes in the microscopic thermodynamics that arise from systematically changing their molecular structure. Therefore, our study provides a blueprint for the strategic syntheses of 2D COFs with "user-defined" electronic and thermal properties that will ultimately aide in their incorporation into various applications.

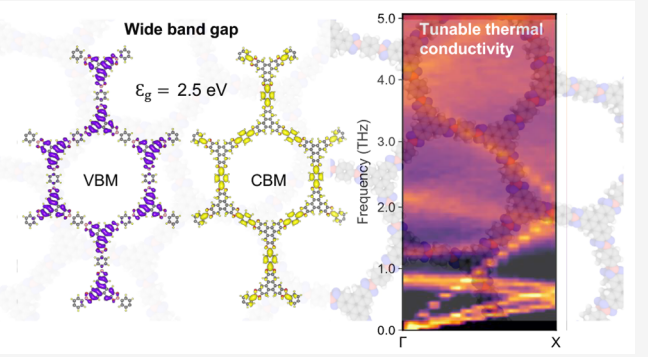


## INTRODUCTION

Recent progress in organic chemistry has led to realizations of novel routes to synthesize tailor-made polymeric semiconductor materials.[1−3] One such emerging class of layered materials are two-dimensional (2D) covalent organic frameworks (COFs) that are constructed by linking light elements with strong covalent bonds.[4−6] Their tunable microstructure with a wide range of selection for the choice of their molecular building block endows them with some exceptional physical attributes.[5,7−13] These physical attributes (which include their high porosities and large surface areas) position them as potential materials for microprocessors,[14] optoelectronics,[15] catalysis,[16,17] gas storage and separation,[18,19] and energy storage[20−22] applications. However, paramount to advancing 2D COFs in these applications is the complete understanding of their electronic and thermal properties. For example, as low-dielectric-constant materials in microprocessors, 2D COFs need to limit the electronic crosstalk and charge buildup, all the while maintaining high heat dissipation ability for high-power-density chips.[14]

In terms of the electronic properties, several studies have elucidated the fundamental relationship between the geometric structure and the electronic structure of 2D polymers in general.[23−35] For instance, it has been shown that by modifying the intrinsic molecular structure, it is possible to change the electronic structure near the Fermi energy from completely flat bands to highly dispersive bands,[25,29] thus offering a route to manipulating the charge carrier mobilities in porous 2D polymers. Interestingly, systematically increasing the linker

Received: January 30, 2023
Revised: May 9, 2023
Published: June 2, 2023

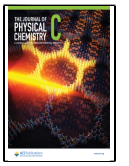




https://doi.org/10.1021/acs.jpcc.3c00652
J. Phys. Chem. C 2023, 127, 11157−11166

lengths in 2D COFs have been shown to decrease the band gaps.[23,27] This has been ascribed to the systematic variations in the valence band maximum (VBM) that are primarily delocalized on the linkers, while the conduction band minimum (CBM) is preferentially localized at the nodes, which are not affected by the linker length variations.[23] Furthermore, the distribution of charge densities and their spatial separation in COFs have also been shown to be critically important for their photocatalytic applications.[36−46] In this regard, Jin et al.[36] have shown that various combinations of nodes and linkers in $sp^2$-carbon COFs can be used to tune the level of VBM and CBM, respectively, thus providing synthetic means to independently modulate the VBM and CBM through manipulating the structures of the nodes and linkers. Likewise, through an end-capping strategy, Yang et al.[41] synthesized vinylene-linked COFs end-capped with hydroxyl groups that showed modular band gaps and improved photocatalytic hydrogen evolution activity. For a thorough review of the optoelectronic properties of COFs, the readers are referred to a recent review conducted by Keller and Bein.[47]

These studies have highlighted the immense potential of 2D COFs with their tailorable electronic properties for optoelectronic applications. However, most studies that have focused on understanding the electronic properties in 2D COFs have generally limited their investigations to one family of COFs (although with systematic changes in the pore geometries), thus making it difficult for a comparative study of the relative effects of different functional groups on the electronic properties. For example, different combinations of functional groups forming the linkers and nodes can be used in different topologies to design a vast array of 2D COFs (inset of Figure 1). Therefore, in this work, we will mainly focus our attention to different families of COFs and how the variations in the functional groups can lead to variations in the electronic structures. Considering the vast possibilities of combining different functional groups into different geometries, we will also limit our calculations to 2D COFs that have been synthesized with the hexagonal topology (as shown in the inset of Figure 1) because this geometry has been the popular choice for synthesizing a variety of 2D COFs with varying porosities.[48] More specifically, we will compare the electronic properties of various families such as imine-, boronate ester-, and azine-based hexagonal 2D COFs and study how their chemical and geometric features can dictate their band gaps, which will ultimately guide the proper engineering of their electronic properties for targeted applications.

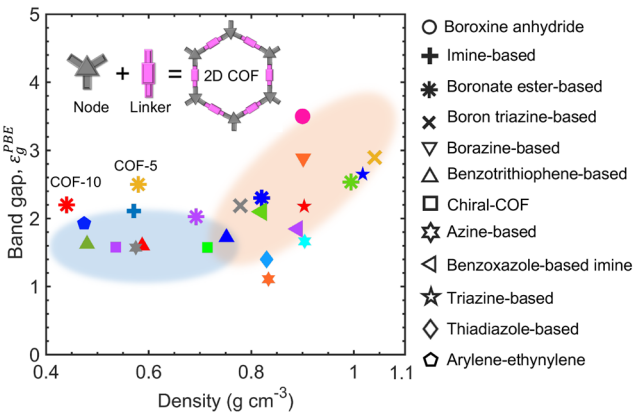


**Figure 1.** Electronic band gap of 24 different 2D COFs with hexagonal lattice as a function of their mass densities. Two different shaded regions in the mass densities illustrate the change in band gap with mass densities of COF structures. No significant change in band gaps is observed within 0.4−0.8 g cm$^{-3}$ (blue shaded region). Although, beyond this limit (orange shaded region) the band gap increases notably with increasing densities (and decreasing porosities). The correlation factor between the band gap and mass densities of COFs in the latter region is ∼0.7. However, for certain COFs with HHTP nodes (such as COF-5 and COF-10), the band gap is larger even though the mass densities are comparatively lower.

In terms of understanding the thermal transport properties in organic framework materials in general, COFs have received far less attention as compared to their metal−organic framework (MOF) cousins.[49−55] Moreover, insights gained from MOFs are not directly transferable to 2D COFs mainly because of their immensely different chemical and structural makeups; where 2D COFs are mainly made up of light atoms held together in a layered van der Waals structure by strong covalent bonds along the layers, MOFs are made up of heavy metallic elements with strong ionic bonding. These differences can lead to drastically different vibrational physics in 2D COFs as compared to MOFs. For instance, it could be expected that the weaker interactions in 2D COFs in the through-plane direction could lead to unprecedented anharmonicity that results in ultralow thermal conductivities via increased phonon scattering.[56] However, we have recently shown that 2D COFs can possess higher overall thermal conductivities as compared to other porous solids with similar densities, mainly due to their periodic structure and light atoms.[13,14] A comparative study of 2D COFs with different motifs and architecture, however, is still lacking and could shed light on the important structural features that dictate heat conduction in these novel 2D materials.

In this work, we study the electronic and thermal properties of 24 different 2D COFs through density functional theory (DFT) calculations and molecular dynamics (MD) simulations. Our DFT-calculated band gaps show that the pore size (or density) is one of the main structural descriptors that controls their band gaps. However, we also identify specific functional groups forming the nodes of 2D COFs that are accompanied by larger band gaps resulting from considerable charge localization. Our equilibrium MD simulations utilizing the Green−Kubo (GK) approach also provide similar results for the thermal conductivity where higher thermal conductivities are generally associated with higher densities of the 2D COFs. Our spectral energy density (SED) calculations also reveal that shorter linkers are associated with greater anharmonicity and increased coupling between acoustic and optical phonons leading to lower thermal conductivities along the 2D planes. However, we also find that functional groups forming relatively larger nodes with more number of covalent bonds connected to the linkers are also associated with higher thermal conductivities along the 2D planes. The resulting changes in physical properties from variations in the building blocks in 2D COFs can lend insights into the connection between the different physical properties that can be attained by systematically changing their molecular building blocks. This will ultimately provide the platform to develop 2D COFs with "user-defined" properties and unrivaled performance in some of the aforementioned applications.


https://doi.org/10.1021/acs.jpcc.3c00652
J. Phys. Chem. C 2023, 127, 11157−11166

## METHODS

**Density Functional Theory (DFT) Calculation.** We perform DFT calculations to predict the electronic band gaps of our COF structures using the commercially available software package, Quantum Espresso.[57,58] Initially, the self-consistent field (SCF) calculation is performed by utilizing the projector augmented wave (PAW) method with the Perdew–Burke–Ernzerhof (PBE) exchange-correlation functional. A uniform $k$-mesh grid of $6 \times 6 \times 1$ is used for our COF structures with the plane-wave basis cutoffs for the wave functions set at 50 Ry. Moreover, to eliminate the interactions of periodic images, a vacuum space of ∼10 Å is created in the through-plane direction of the COF layers, which is consistent with prior works that have performed a similar approach to remove any image effects that lead to large electron–electron repulsions from the images.[23,24] We note that, in general, DFT calculations have been shown to underpredict the electronic band gaps. As such, our calculations should be taken as lower bounds to the actual band gaps of the COFs. However, as the main purpose of our work is a comparative study between the different 2D COFs, the choice of the same exchange correlation functional and our DFT approach should suffice for our purposes.

**Molecular Dynamics (MD) Simulations.** We perform MD simulations on our 2D COF structures by utilizing the Adaptive Intermolecular Reactive Empirical Bond Order (AIREBO) potential widely used for simulating hydrocarbons.[59−61] To show the generality of the results presented in this work, we also perform calculations with a Universal Force Field (UFF) all-atom potential[62] that can parametrize different funcitonal groups in the 2D COFs. For all our MD simulations, we use the Large-scale Atomic/Molecular Massively Parallel Simulator (LAMMPS) package.[63] For our equilibration process, the COF structures are initially equilibrated at ambient pressure for 2 ns with a time step of 0.5 fs under the Nosé–Hoover thermostat and barostat (NPT) ensemble, where the number of particles, pressure and temperature are kept constant throughout the equilibration process.[64] Following the NPT integration, we further equilibrate our structures for 1 ns under the NVT ensemble where the number of particles, volume, and temperature are held constant. Next, we use the NVE ensemble (where number of particles, volume, and total energy of the system are kept constant) for an additional equilibration for 1 ns. For the entire simulation, we use periodic boundary conditions in all the three principal directions. Finally, we utilize the GK formalism to calculate the thermal conductivities of our 2D COF domains.

We note that we calculate the thermal conductivities of monolayer 2D COFs and as such report the in-plane thermal conductivities. To predict the in-plane thermal conductivities of our 2D COF structures, we utilize the GK formalism under the equilibrium molecular dynamics (EMD) simulations framework. In this method, the thermal conductivity is calculated as[61,65−69]

$$\kappa_{x,y} = \frac{1}{k_B V T^2} \int_0^\infty \langle J_{x,y}(t) J_{x,y}(0) \rangle \, \mathrm{d}t \tag{1}$$

where $V$, $T$, and $t$ are the volume of the system, temperature, and time, respectively, and $\langle J_{x,y}(t) J_{x,y}(0) \rangle$ is the component of the heat current autocorrelation function (HCACF) along the $x$- or $y$-directions, which is calculated as[70]

$$\mathbf{J} = \frac{1}{V} \left( \sum_i \mathbf{v}_i \epsilon_i + \sum_i \mathbf{S}_i \cdot \mathbf{v}_i \right) \tag{2}$$

where $\mathbf{v}_i$, $\epsilon_i$, and $\mathbf{S}_i$ are the velocity, energy and stress of atom $i$, respectively. Our calculations (as presented below) show that the in-plane thermal conductivities in the $x$- and $y$-directions are similar, and therefore we only report an average value for the in-plane thermal conductivities of our 2D COFs. To account for the cell size effects in the thermal conductivity calculations, we calculated the thermal conductivities for varying cell sizes, which are shown in Figures S3 and S4. Finally, we choose a domain length of ∼120 Å along the in-plane direction, as convergence of thermal conductivity is achieved beyond this length.

**Phonon Spectral Energy Density (SED) Calculation.** We calculate the phonon dispersion curves of our COF structures by calculating the SED as a function of wave vector ($\mathbf{q}$) and frequency ($\omega$), in our MD simulations, which is calculated as[71,72]

$$\Phi(\mathbf{q}, \omega) = \frac{1}{4\pi\tau N_T} \times \sum_\alpha^3 \sum_b^B m_b \left| \int_0^\tau \sum_{n_{x,y,z}}^{N_T} \dot{u}_\alpha^{n_{x,y,z},b}(t) \exp[i\mathbf{q} \cdot r^{n_{x,y,z},b=0} - i\omega t] \, \mathrm{d}t \right|^2 \tag{3}$$

where $\tau$ is the total simulation time, $\alpha$ is the Cartesian direction, $n_{x,y,z}$ is a unit cell, $N_T$ is the number of unit cells in the crystal, $b$ is the atom label in a given unit cell, $B$ is the atomic number in the unit cell, $m_b$ is the mass of atom $b$ in the unit cell, and $\dot{u}_\alpha^{n_{x,y,z},b}(t)$ denotes the velocity of the $b^{\text{th}}$ atom in the $n^{\text{th}}$ unit cell along the $\alpha$ direction at time $t$.

For our SED calculations, we construct the computational domain of our COF structures with total number of unit cells, $N_T = 200$. Next, we equilibrate our COF supercell structure initially under the Nosé–Hoover thermostat and barostat (i.e., the NPT ensemble)[64] for 2 ns with a time step of 0.5 fs where the number of particles, pressure, and temperature of the system are kept constant at 0 bar pressure. Following the NPT integration, we further equilibrate our structures under the NVT ensemble where the volume and temperature are held constant for a total of 2 ns. Finally, for the data collection for our SED calculation, we output the velocities and positions of each atoms using the microcanonical ensemble (or NVE ensemble) for 1.5 ns.

## RESULTS AND DISCUSSION

Figure 1 shows our DFT-calculated band gaps for the hexagonal 2D COFs studied in this work. The details of our calculations are given in the Methods section, and the chemical structures for all our 2D COFs are provided in the Supporting Information. Overall, the band gaps of 2D COFs are larger for higher densities (lower porosities) with a few exceptions that possess relatively larger band gaps at low mass densities (such as COF-5) or lower band gaps at intermediate densities (such as the azine-based ACOF-1). The calculated band gaps are also rather independent of mass density for the 0.4–0.8 g cm$^{-3}$ range (as highlighted by the blue shaded region in Figure 1). However, as density is increased further, there is a clear evidence of increasing band gap with increasing density (for >0.8 g cm$^{-3}$ as highlighted by the orange shaded region in Figure 1). To quantify this relationship between the band gap



https://doi.org/10.1021/acs.jpcc.3c00652
J. Phys. Chem. C 2023, 127, 11157−11166

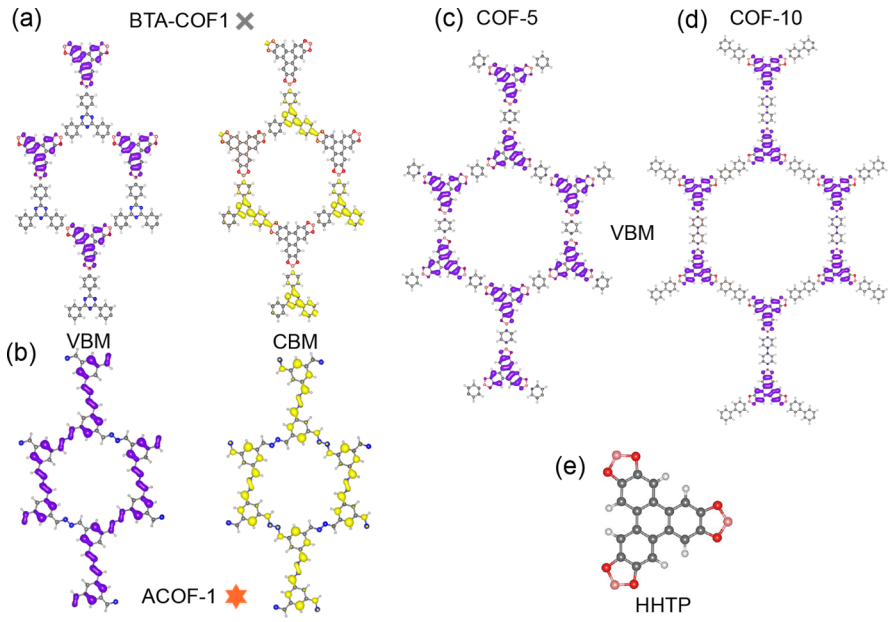


**Figure 2.** Electronic charge densities showing spatial separation between the valence band maximum (VBM) and conduction band minimum (CBM) for (a) BTA-COF1, (b) ACOF-1, (c) COF-5, and (d) COF-10. The HHTP nodes (e) in BTA-COF-1, COF-5, and COF-10 localize the VBM, whereas in ACOF-1, the spatial localization is absent, which results in the lower band gap as compared to the other COFs with the HHTP node.

and mass density for the second region (>0.8 g $cm^{-3}$), we fit a correlation coefficient of ∼0.7, which demonstrates a moderately well represented relationship between the band gap of COFs and their mass densities for this regime. This increase in band gap with mass density is consistent with prior works that have shown that band gap monotonically decreases with increasing linker length (albeit for COFs with the same functional groups unlike in our study).[23,26,28] Therefore, our band gap calculations show that along with the mass densities of COFs the functional group can also significantly dictate their electronic band gaps.

To better explain the overall trend, we calculate the partial charge densities for the VBM and the CBM for our 2D COFs as shown in Figure 2 for some representative COFs. Interestingly, we find considerable spatial separation of the charge densities for majority of COFs that possess large band gaps as represented by BTA-COF1 (Figure 2a). Whereas for COFs with relatively lower band gaps (even at intermediate mass densities), we find that the charge densities for the CBM and VBM are mostly delocalized throughout the COF structure and are spatially overlapping (as shown for ACOF-1 in Figure 2b). In most cases, we find that the imine functional group at the linker as shown in Figure 2b for ACOF-1 is associated with delocalization of charge densities (see also Figure S2 for COFs with imine functional groups that have delocalized charge densities). Furthermore, for COF-5 and COF-10 (with the wider band gaps at relatively low densities as shown in Figure 1), we also find considerable localization of the charge densities (see Figures 2c,d). It has been previously shown that confinement or localization of charge densities plays a significant role in dictating the band gaps of 2D COFs.[23,24] For example, with reduction in quantum confinement in TP-COF (with a larger porosity) as compared to COF-5, the band gap decreases considerably in TP-COF.[24] The reduction in quantum confinement results in a more delocalized nature of the charge density of VBM for TP-COF. Similarly, in our charge density calculations, we find that majority of the COFs with large band gaps exhibit significant localization of spatial distribution of charge densities. This suggests that localization of charge densities can result in wider band gaps in 2D COFs. Considering the chemical structure of the COFs, it becomes evident that the localized nature of charge densities is mostly related to COFs with the HHTP (2,3,6,7,10,11-hexahydroxytriphenylene) node (Figure 2e). This suggests that COFs with HHTP functional group forming the nodes can possess wider band gaps even at low mass densities. Note, as the VBM−CBM gaps are inherently tied to energy conversion efficiencies and are particularly beneficial in photovoltaic application,[73,74] a strategy to manipulate the physical charge separation could be to use HHTP nodes with longer linkers to maximize charge separation and increase band gap. Overall, our partial charge density calculations together with our band gap calculations show that the localized nature of the electronic charge densities can result in wider band gaps in 2D COFs, and this can be manipulated via the strategic choice of both the node and the linker in the 2D COFs. This also has major implications for the formation of excitons because the generation of electrons and holes will be localized at different spatial positions in the COF sublattice such as in the case for BTA-COF1, COF-5, or COF-10 as shown in Figure 2.

Next, to gain more insights into engineering the electronic properties of COFs, we compare the chemical structures of COFs with similar densities but drastically varying band gaps. For example, we compare the chemical structure and the electronic properties of the boronate ester-based and the azine-based COFs at 0.9 g $cm^{-3}$ as shown in Figure 1. We find that the imine functional groups forming the linkers are mainly associated with lower band gaps. As mentioned in our previous discussion, the imine groups are also associated with the delocalization of the electron densities that reduce the band gap. Thus, adopting the materials by design strategy, we now


https://doi.org/10.1021/acs.jpcc.3c00652
J. Phys. Chem. C 2023, 127, 11157−11166

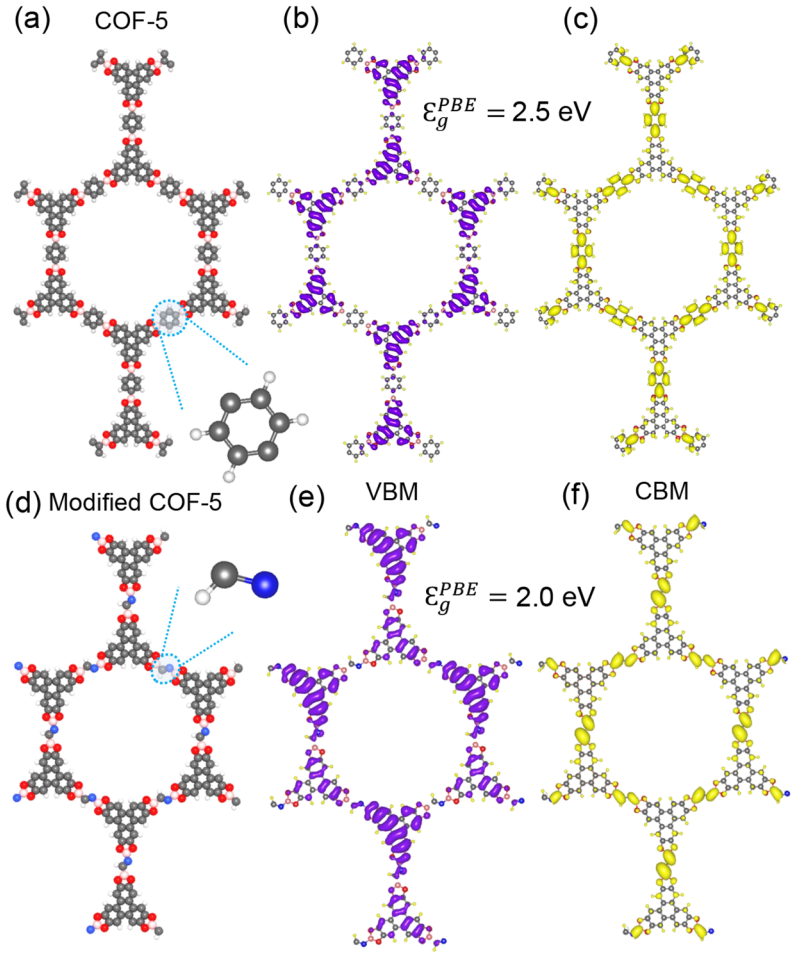


**Figure 3.** Schematic of the chemical structure (a), charge densities of VBM (b), and CBM (c) for COF-5. Schematic of the chemical structure (d), charge densities of VBM (e), and CBM (f) for our modified COF-5 where the linker is replaced with the imine functional group. The modified COF-5 possesses a lower band gap resulting from the greater delocalization of the charge densities.

attempt to modify the band gap without drastically varying the mass densities (or network porosities) because the approach of varying mass density to manipulate the band gap has already been established from prior works, albeit for the same family of COFs.[23,26,28] To this end, we replace the benzene linker in the 2D COF-5 structure possessing the relatively higher band gap, with the imine functional linker. The goal behind this strategy is to decrease the band gap via delocalizing the spatially localized electron densities around the HHTP nodes in COF-5. As shown in Figures 3a–c, the HHTP node in COF-5 is where the VBM orbitals are localized, whereas the CBM are spatially separated and mainly located around the linkers. However, when the benzene linkers are replaced with the imine functional group in the modified COF-5 (see Figures 3d–f), the VBM are delocalized from the HHTP nodes, thus spatially overlapping with the CBM orbitals. This also leads to a reduction in the band gap from 2.5 eV in the original COF-5 to 2 eV in the modified COF-5 structure, which demonstrates the ability of the imine linkers to effectively lower the band gap through increasing the charge density delocalization. Note that the stability of the modified COF-5 structure has been confirmed by our DFT calculations as detailed in the Supporting Information.

To put our results of the electronic calculations for our 2D COFs into a broader perspective, we can compare the modular band gaps that we calculate to other technologically relevant materials such as graphene. Although graphene, a similar layered material, has shown great promise for next-generation technologies, its near-zero band gap limits its practical use in electronic devices. In this regard, 2D COFs offer the unique platform where these materials can combine the advantages of 2D material systems (such as quantum confinement effects) with the modular and wide band gaps that are highly desirable for important applications such as in high-power, high-frequency electronics. Furthermore, the larger band gaps (>2 eV) for 2D COFs with mass densities >0.9 g $cm^{-3}$ and for lower density COFs with the HHTP nodes (Figure 1) are on par with some of the widely used fully inorganic wide band gap semiconductors such as SiC (with band gaps in the range 2.3–3.3 eV).[75] Thus, along with their low dielectric constants,[14] the wide and tunable band gaps of 2D COFs position these materials as prime candidates for organic field-effect transistors where electronic crosstalk needs to be minimized.

We now turn our focus to the thermal properties of 2D COFs. Because DFT-based calculations of thermal conductivity by solving the full Boltzmann transport equation for these 2D COFs with large unit cells are computationally very expensive, we instead utilize MD simulations to calculate their thermal conductivities. For this, we use the AIREBO potential to describe the interatomic interactions in our COFs.[76] We note that as the full parametrization of all the varying atomic species (such as boron, oxygen, and nitrogen) has not been


https://doi.org/10.1021/acs.jpcc.3c00652
J. Phys. Chem. C 2023, 127, 11157–11166

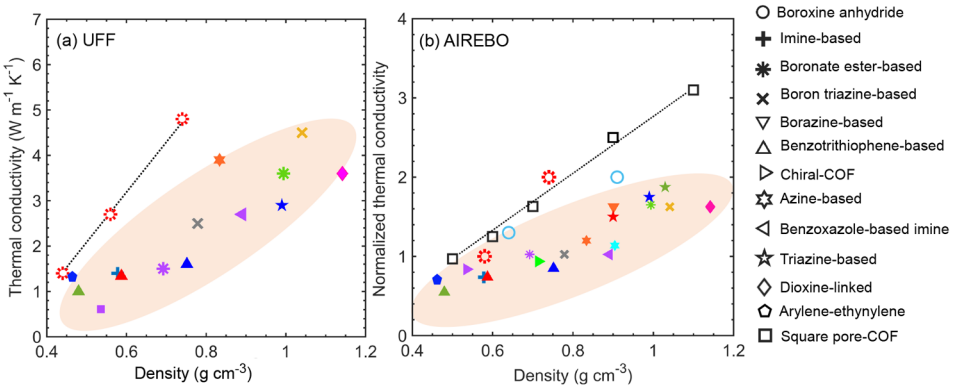


**Figure 4.** (a) In-plane thermal conductivities of our 2D COFs calculated using the UFF potential and (b) normalized in-plane thermal conductivities (with respect to the in-plane thermal conductivity of the prototypical 2D COF-5) calculated using the AIREBO potential as a function of mass densities. In both cases the thermal conductivity monotonically increases with increasing mass densities and decreasing porosities. Although quantitative thermal conductivities are different between the two potentials, the "all-carbon" AIREBO models and the 2D COFs modeled by using the UFF potential that includes all interactions between the different atoms show similar trends in the in-plane thermal conductivity; both potentials demonstrate higher in-plane thermal conductivities for COFs with relatively larger nodes (such as that for the boronate ester-based COFs) as highlighted by the dashed lines.

implemented in the AIREBO potential, we base our calculations for the different COFs with all carbon atoms. As such, although the quantitative values of thermal conductivities could be different than that of the actual COF structures (with a better potential that includes the complete parametrization for all atoms), we can utilize the knowledge gained from our thermal property calculations from MD simulations to qualitatively compare the results between the different COFs studied in this work. This allows us to modify the linker size (or porosity) while keeping everything else (such as the interaction parameters between all atoms and the functional groups of the linkers) the same, thus providing a clear assessment of the effect of porosity on their thermal conductivities. However, we also conduct thermal conductivity calculations for our 2D COFs with the use of the UFF potential to gauge the generality of the trends in thermal conductivity calculations as we discuss in more detail below. We note that we could only parametrize 16 out of the 24 COFs with the UFF potential because we could not find all the parameters of the atomic interactions for some COFs (such as that for our square lattice COF as mentioned below). However, both potentials show similar trends in the in-plane thermal conductivities of the 2D COFs with density, which not only provides confidence in our calculations but also provides further support for the generality of the conclusions made in the following discussions for 2D COFs.

Figures 4a and 4b show the in-plane thermal conductivities of our 2D COFs calculated with the UFF and AIREBO potentials, respectively. We note that for the AIREBO potential we plot the in-plane thermal conductivity of our COFs normalized with respect to the in-plane thermal conductivity of the prototypical COF-5 structure as a function of their mass densities. This is because we are more interested in the qualitative results of heat transfer in these structures that represent "toy models" with all carbon atoms, rather than predicting material specific quantitative values. In contrast, the UFF potential has all-atom parametrization, which can differentiate between the different functional groups and atom types in the various 2D COFs, and so we present the quantitative values of the in-plane thermal conductivities for our 2D COFs in Figure 4a. There are two aspects of the data (calculated with both UFF and AIREBO potentials) worth noting from our thermal conductivity results as presented in Figure 4. First, similar to the qualitative increase in the band gap, we also find that, overall, the thermal conductivities increase with increasing mass densities for both the UFF and AIREBO potentials. Second, and probably the more interesting aspect, is the relatively larger increase for a few COFs with increasing mass densities (as highlighted by the dashed line in Figures 4a and 4b for the UFF- and AIREBO-based calculations, respectively).

The first aspect as mentioned above is expected given the fact that thermal conductivity typically scales with increasing atomic density in solids.[77,78] For our COFs, the increased phonon scattering at the larger pores of the lower density COFs is expected to lower thermal conductivities in these materials. To show this more quantitatively, we present the SED calculations (for our COFs based on the COF-1 structure as modeled with the AIREBO potential). Additional details of the SED technique are given in the Methods section. Briefly, the SED calculations provide insight into the anharmonic phonon dispersion relations and lifetimes directly from the velocities of the atoms in the computational domain.[79] Thus, it incorporates the full temperature-dependent anharmonicity differently than typical lattice dynamics calculations used for thermal conductivity calculations that only include three-phonon scattering events and neglect the higher-order phonon scattering that become increasingly important for anharmonic materials such as COFs, as we point out below.

We compare the SED for the COFs with varying porosities but with similar functional groups (exclusively with all-carbon and hydrogen atoms) forming the nodes and linkers as shown in Figures 5a and 5b. Note that we have increased the linker length by adding a benzene ring to the COF-1 structure, thus allowing us to only consider the effect of porosity and not variations in functional groups that can affect thermal conductivity. Figures 5c and 5d show our SED calculations for the lower and higher density COFs based on the COF-1 structure. The higher contrast in the shading of the plot (relating to the higher magnitude of SEDs) indicates that the modes have higher kinetic energies. As such, the higher SEDs along with the increase in their broadening suggest that, on


https://doi.org/10.1021/acs.jpcc.3c00652
J. Phys. Chem. C 2023, 127, 11157−11166

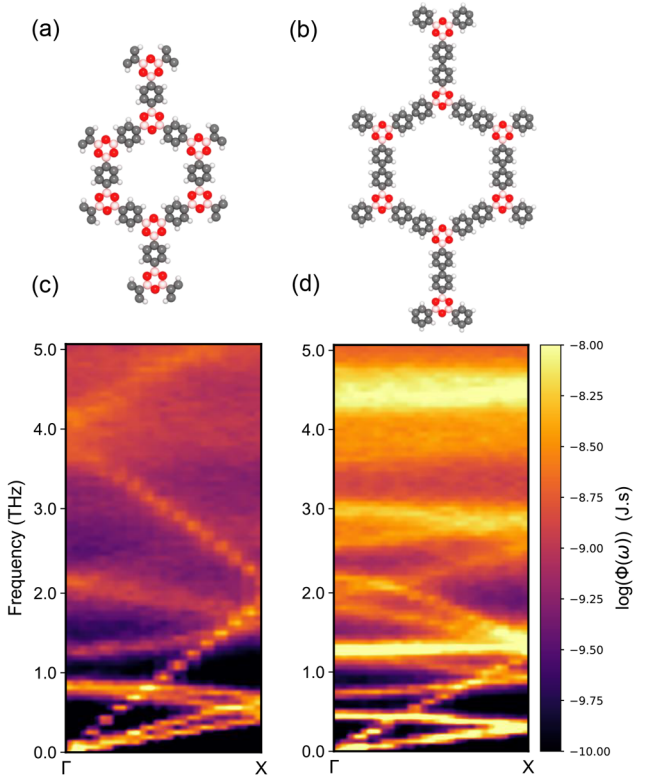


**Figure 5.** Schematics of the (a) COF-1 and (b) COF-1-2R (modified COF-1 with increased linker length) structures. Calculations of their spectral energy densities in (c) and (d), respectively, show that the longer linker lengths are associated with increased anharmonicities and stronger coupling between the heat carrying acoustic modes and the optic modes.

average, the vibrational modes in the longer linkers experience stronger anharmonicity and vibrational scattering with shorter vibrational lifetimes. For the longer linker case, our SED calculations show a loss of definition of the wave vectors for frequencies higher than ∼2 THz. It is also interesting to note that the flatter bands with reduced group velocities are introduced throughout the spectrum, demonstrating the coupling of optical modes with heat carrying acoustic modes that result in reduced thermal conductivities for these materials. For example, we predict the thermal conductivity of ∼4 W $m^{-1}$ $K^{-1}$ for COF-1 along the 2D plane, which is 3 orders of magnitude lower than that of graphene.

The second aspect worth noting in Figure 4 where we find relatively higher increase for a few COFs with increasing mass densities can be ascribed to the larger nodes of the COFs. As shown in Figure 4, the combination of lower densities and lower thermal conductivities is associated with COFs that have relatively smaller nodes (see Figures S1 and S2). However, replacing the nodes with bigger functional groups (as demonstrated by the four-arm COF in Figure 4 whose molecular structure is presented in Figure S9), we can increase the thermal conductivity by 2-fold in these materials. Comparison of SED calculations for similar mass density COFs but with varying node sizes suggests that the bigger nodes with more covalent bonds connecting the nodes to the linkers are associated with lower anharmonicities (Figure S6), which is consistent with their relatively higher thermal conductivities. Furthermore, systematically changing the linker length, as presented for the square COF (hollow square symbols in Figure 4), can be utilized to vary the thermal conductivity by more than 2-fold. Therefore, our MD simulations show that 2D COFs with larger nodes provide a better platform to engineer their thermal conductivities across a wider range.

## CONCLUSIONS

Our DFT calculations of electronic properties and MD simulations of thermal conductivity have shown that one of the main factors dictating the physical properties of 2D COFs is their porosity. However, with the proper choice of the functional group, such as COFs with the relatively larger HHTP nodes that are associated with higher thermal conductivities and larger band gaps, these physical properties can be modulated across a wide range. For their electronic properties, the localization of charge densities can be varied based on the functional groups, which can result in spatially separated valence and conduction bands. This has major implications for exciton formation and photovoltaic applications of 2D COFs. For their thermal properties, larger nodes and shorter linkers are associated with reduced anharmonicity (and lesser coupling between the heat carrying acoustic modes and the optic modes) in these materials, which result in relatively higher thermal conductivities. Moreover, 2D COFs with larger nodes provide a wider range for thermal conductivity modulation with variation in their porosities. Taken together, our work demonstrates that 2D COFs are a novel class of multifunctional materials that provide the platform for "user-defined" physical properties based on the choice of their molecular building block. The fundamental mechanistic understanding presented in this work will help guide the future syntheses of these new classes of modular and periodic 2D polymer networks for targeted applications.

## ASSOCIATED CONTENT

### Supporting Information

The Supporting Information is available free of charge at https://pubs.acs.org/doi/10.1021/acs.jpcc.3c00652.

Details of the two-dimensional organic framework molecular structures, computational domain setup, nonequilibrium molecular dynamics approach, vibrational density of states calculations (PDF)

## AUTHOR INFORMATION

### Corresponding Author

**Ashutosh Giri** − *Department of Mechanical, Industrial and Systems Engineering, University of Rhode Island, Kingston, Rhode Island 02881, United States;* orcid.org/0000-0002-8899-4964; Email: ashgiri@uri.edu

### Authors

**Muhammad A. Rahman** − *Department of Mechanical, Industrial and Systems Engineering, University of Rhode Island, Kingston, Rhode Island 02881, United States*

**Sandip Thakur** − *Department of Mechanical, Industrial and Systems Engineering, University of Rhode Island, Kingston, Rhode Island 02881, United States;* orcid.org/0000-0002-3763-3659

**Patrick E. Hopkins** − *Department of Mechanical and Aerospace Engineering, University of Virginia, Charlottesville, Virginia 22904, United States;* orcid.org/0000-0002-3403-743X



https://doi.org/10.1021/acs.jpcc.3c00652
J. Phys. Chem. C 2023, 127, 11157−11166

Complete contact information is available at:
https://pubs.acs.org/10.1021/acs.jpcc.3c00652

### Notes

The authors declare no competing financial interest.

## ■ ACKNOWLEDGMENTS

This work was supported by the Office of Naval Research, Grant Nos. N00014-21-1-2622 and N00014-20-1-2686. The work is also partially supported by the National Science Foundation (NSF Award No. 2119365).

## ■ REFERENCES

(1) Evans, A. M.; Strauss, M. J.; Corcos, A. R.; Hirani, Z.; Ji, W.; Hamachi, L. S.; Aguilar-Enriquez, X.; Chavez, A. D.; Smith, B. J.; Dichtel, W. R. Two-Dimensional Polymers and Polymerizations. *Chem. Rev.* **2022**, *122*, 442−564.
(2) Frey, H.; Johann, T. Celebrating 100 years of "polymer science": Hermann Staudinger's 1920 manifesto. *Polym. Chem.* **2020**, *11*, 8−14.
(3) Lutz, J.-F. 100th Anniversary of Macromolecular Science Viewpoint: Toward Artificial Life-Supporting Macromolecules. *ACS Macro Lett.* **2020**, *9*, 185−189.
(4) Evans, A. M.; Parent, L. R.; Flanders, N. C.; Bisbey, R. P.; Vitaku, E.; Kirschner, M. S.; Schaller, R. D.; Chen, L. X.; Gianneschi, N. C.; Dichtel, W. R. Seeded growth of single-crystal two-dimensional covalent organic frameworks. *Science* **2018**, *361*, 52−57.
(5) Bisbey, R. P.; Dichtel, W. R. Covalent Organic Frameworks as a Platform for Multidimensional Polymerization. *ACS Central Science* **2017**, *3*, 533−543.
(6) Diercks, C. S.; Yaghi, O. M. The atom, the molecule, and the covalent organic framework. *Science* **2017**, *355*, No. eaal1585.
(7) Servalli, M.; Schlüter, A. D. Synthetic Two-Dimensional Polymers. *Annu. Rev. Mater. Res.* **2017**, *47*, 361−389.
(8) Grill, L.; Dyer, M.; Lafferentz, L.; Persson, M.; Peters, M. V.; Hecht, S. Nano-architectures by covalent assembly of molecular building blocks. *Nat. Nanotechnol.* **2007**, *2*, 687.
(9) Waller, P. J.; Lyle, S. J.; Osborn Popp, T. M.; Diercks, C. S.; Reimer, J. A.; Yaghi, O. M. Chemical Conversion of Linkages in Covalent Organic Frameworks. *J. Am. Chem. Soc.* **2016**, *138*, 15519−15522.
(10) Lohse, M. S.; Stassin, T.; Naudin, G.; Wuttke, S.; Ameloot, R.; De Vos, D.; Medina, D. D.; Bein, T. Sequential Pore Wall Modification in a Covalent Organic Framework for Application in Lactic Acid Adsorption. *Chem. Mater.* **2016**, *28*, 626−631.
(11) Côté, A. P.; Benin, A. I.; Ockwig, N. W.; O'Keeffe, M.; Matzger, A. J.; Yaghi, O. M. Porous, Crystalline, Covalent Organic Frameworks. **2005**, *310*, 1166−1170.
(12) Xu, H.; Gao, J.; Jiang, D. Stable, crystalline, porous, covalent organic frameworks as a platform for chiral organocatalysts. *Nat. Chem.* **2015**, *7*, 905.
(13) Giri, A.; Evans, A. M.; Rahman, M. A.; McGaughey, A. J. H.; Hopkins, P. E. Highly Negative Poisson's Ratio in Thermally Conductive Covalent Organic Frameworks. *ACS Nano* **2022**, *16*, 2843.
(14) Evans, A. M.; Giri, A.; Sangwan, V. K.; Xun, S.; Bartnof, M.; Torres-Castanedo, C. G.; Balch, H. B.; Rahn, M. S.; Bradshaw, N. P.; Vitaku, E.; et al. Thermally conductive ultra-low-k dielectric layers based on two-dimensional covalent organic frameworks. *Nat. Mater.* **2021**, *20*, 1142.
(15) Facchetti, A. pi-Conjugated Polymers for Organic Electronics and Photovoltaic Cell Applications. *Chem. Mater.* **2011**, *23*, 733−758.
(16) Wang, S.; Sun, Q.; Chen, W.; Tang, Y.; Aguila, B.; Pan, Y.; Zheng, A.; Yang, Z.; Wojtas, L.; Ma, S.; et al. Programming Covalent Organic Frameworks for Photocatalysis: Investigation of Chemical and Structural Variations. *Matter* **2020**, *2*, 416−427.
(17) Ding, S.-Y.; Gao, J.; Wang, Q.; Zhang, Y.; Song, W.-G.; Su, C.-Y.; Wang, W. Construction of Covalent Organic Framework for Catalysis: Pd/COF-LZU1 in Suzuki−Miyaura Coupling Reaction. *J. Am. Chem. Soc.* **2011**, *133*, 19816−19822.
(18) Han, S. S.; Furukawa, H.; Yaghi, O. M.; Goddard, W. A. Covalent Organic Frameworks as Exceptional Hydrogen Storage Materials. *J. Am. Chem. Soc.* **2008**, *130*, 11580−11581.
(19) Lohse, M. S.; Bein, T. Covalent Organic Frameworks: Structures, Synthesis, and Applications. *Adv. Funct. Mater.* **2018**, *28*, 1705553.
(20) Romero, J.; Rodriguez-San-Miguel, D.; Ribera, A.; Mas-Ballesté, R.; Otero, T. F.; Manet, I.; Licio, F.; Abellán, G.; Zamora, F.; Coronado, E. Metal-functionalized covalent organic frameworks as precursors of supercapacitive porous N-doped graphene. *J. Mater. Chem. A* **2017**, *5*, 4343−4351.
(21) DeBlase, C. R.; Silberstein, K. E.; Truong, T.-T.; Abruña, H. D.; Dichtel, W. R. Beta-Ketoenamine-Linked Covalent Organic Frameworks Capable of Pseudocapacitive Energy Storage. *J. Am. Chem. Soc.* **2013**, *135*, 16821−16824.
(22) Santiago-Maldonado, X. Covalent organic framework-based electrolytes fabricated for solid-state Li-ion batteries. *MRS Bull.* **2021**, *46*, 1006.
(23) Zhu, P.; Meunier, V. Electronic properties of two-dimensional covalent organic frameworks. *J. Chem. Phys.* **2012**, *137*, 244703.
(24) Zhou, Y.; Wang, Z.; Yang, P.; Zu, X.; Gao, F. Electronic and optical properties of two-dimensional covalent organic frameworks. *J. Mater. Chem.* **2012**, *22*, 16964−16970.
(25) Adjizian, J.-J.; Briddon, P.; Humbert, B.; Duvail, J.-L.; Wagner, P.; Adda, C.; Ewels, C. Dirac Cones in two-dimensional conjugated polymer networks. *Nat. Commun.* **2014**, *5*, 5842.
(26) Liang, L.; Zhu, P.; Meunier, V. Electronic, structural, and substrate effect properties of single-layer covalent organic frameworks. *J. Chem. Phys.* **2015**, *142*, 184708.
(27) Gutzler, R.; Perepichka, D. F. pi-Electron Conjugation in Two Dimensions. *J. Am. Chem. Soc.* **2013**, *135*, 16585−16594.
(28) Gutzler, R. Band-structure engineering in conjugated 2D polymers. *Phys. Chem. Chem. Phys.* **2016**, *18*, 29092−29100.
(29) Alcón, I.; Viñes, F.; Moreira, I. d. P. R.; Bromley, S. T. Existence of multi-radical and closed-shell semiconducting states in post-graphene organic Dirac materials. *Nat. Commun.* **2017**, *8*, 1957.
(30) Thomas, S.; Li, H.; Zhong, C.; Matsumoto, M.; Dichtel, W. R.; Bredas, J.-L. Electronic Structure of Two-Dimensional pi-Conjugated Covalent Organic Frameworks. *Chem. Mater.* **2019**, *31*, 3051−3065.
(31) Thomas, S.; Li, H.; Dasari, R. R.; Evans, A. M.; Castano, I.; Allen, T. G.; Reid, O. G.; Rumbles, G.; Dichtel, W. R.; Gianneschi, N. C.; et al. Design and synthesis of two-dimensional covalent organic frameworks with four-arm cores: prediction of remarkable ambipolar charge-transport properties. *Mater. Horiz.* **2019**, *6*, 1868−1876.
(32) Raptakis, A.; Croy, A.; Dianat, A.; Gutierrez, R.; Cuniberti, G. Exploring the similarity of single-layer covalent organic frameworks using electronic structure calculations. *RSC Adv.* **2022**, *12*, 12283−12291.
(33) Merkel, K.; Greiner, J.; Ortmann, F. Understanding the electronic pi-system of 2D covalent organic frameworks with Wannier functions. *Sci. Rep.* **2023**, *13*, 1685.
(34) Patwardhan, S.; Kocherzhenko, A. A.; Grozema, F. C.; Siebbeles, L. D. A. Delocalization and Mobility of Charge Carriers in Covalent Organic Frameworks. *J. Phys. Chem. C* **2011**, *115*, 11768−11772.
(35) Pham, H. Q.; Le, D. Q.; Pham-Tran, N.-N.; Kawazoe, Y.; Nguyen-Manh, D. Electron delocalization in single-layer phthalocyanine-based covalent organic frameworks: a first principle study. *RSC Adv.* **2019**, *9*, 29440−29447.
(36) Jin, E.; Geng, K.; Fu, S.; Addicoat, M. A.; Zheng, W.; Xie, S.; Hu, J.-S.; Hou, X.; Wu, X.; Jiang, Q.; et al. Module-Patterned Polymerization towards Crystalline 2D sp2-Carbon Covalent Organic Framework Semiconductors. *Angew. Chem., Int. Ed.* **2022**, *61*, No. e202115020.
(37) Chen, Z.; Wang, J.; Hao, M.; Xie, Y.; Liu, X.; Yang, H.; Waterhouse, G. I. N.; Wang, X.; Ma, S. Tuning excited state electronic

structure and charge transport in covalent organic frameworks for enhanced photocatalytic performance. *Nat. Commun.* **2023**, *14*, 1106.
(38) Chen, R.; Wang, Y.; Ma, Y.; Mal, A.; Gao, X.-Y.; Gao, L.; Qiao, L.; Li, X.-B.; Wu, L.-Z.; Wang, C. Rational design of isostructural 2D porphyrin-based covalent organic frameworks for tunable photocatalytic hydrogen evolution. *Nat. Commun.* **2021**, *12*, 1354.
(39) Wang, X.; Chen, L.; Chong, S. Y.; Little, M. A.; Wu, Y.; Zhu, W.-H.; Clowes, R.; Yan, Y.; Zwijnenburg, M. A.; Sprick, R. S.; et al. Sulfone-containing covalent organic frameworks for photocatalytic hydrogen evolution from water. *Nat. Chem.* **2018**, *10*, 1180−1189.
(40) Li, C.; Liu, J.; Li, H.; Wu, K.; Wang, J.; Yang, Q. Covalent organic frameworks with high quantum efficiency in sacrificial photocatalytic hydrogen evolution. *Nat. Commun.* **2022**, *13*, 2357.
(41) Yang, Y.; Chu, X.; Zhang, H.-Y.; Zhang, R.; Liu, Y.-H.; Zhang, F.-M.; Lu, M.; Yang, Z.-D.; Lan, Y.-Q. Engineering beta-ketoamine covalent organic frameworks for photocatalytic overall water splitting. *Nat. Commun.* **2023**, *14*, 593.
(42) Li, S.; Ma, R.; Xu, S.; Zheng, T.; Wang, H.; Fu, G.; Yang, H.; Hou, Y.; Liao, Z.; Wu, B.; et al. Two-Dimensional Benzobisthiazole-Vinylene-Linked Covalent Organic Frameworks Outperform One-Dimensional Counterparts in Photocatalysis. *ACS Catal.* **2023**, *13*, 1089−1096.
(43) Chen, R.; Shi, J.-L.; Ma, Y.; Lin, G.; Lang, X.; Wang, C. Designed Synthesis of a 2D Porphyrin-Based sp2 Carbon-Conjugated Covalent Organic Framework for Heterogeneous Photocatalysis. *Angew. Chem., Int. Ed.* **2019**, *58*, 6430−6434.
(44) Yang, C.; Qian, C.; Yu, M.; Liao, Y. Manipulation of band gap and hydrophilicity in vinylene-linked covalent organic frameworks for improved visible-light-driven hydrogen evolution by end-capping strategy. *Chem. Eng. J.* **2023**, *454*, 140341.
(45) Li, Z.; Deng, T.; Ma, S.; Zhang, Z.; Wu, G.; Wang, J.; Li, Q.; Xia, H.; Yang, S.-W.; Liu, X. Three-Component Donor-pi-Acceptor Covalent-Organic Frameworks for Boosting Photocatalytic Hydrogen Evolution. *J. Am. Chem. Soc.* **2023**, *145* (15), 8364−8374.
(46) Gu, Z.; Shan, Z.; Wang, Y.; Wang, J.; Liu, T.; Li, X.; Yu, Z.; Su, J.; Zhang, G. Tuning the exciton binding energy of covalent organic frameworks for efficient photocatalysis. *Chin. Chem. Lett.* **2023**, 108356.
(47) Keller, N.; Bein, T. Optoelectronic processes in covalent organic frameworks. *Chem. Soc. Rev.* **2021**, *50*, 1813−1845.
(48) Wang, Y.; Wang, G.; Liu, Y.; Zheng, B.; Wang, Z.; Yang, Q. Identifying Promising Covalent-Organic Frameworks for Decarburization and Desulfurization from Biogas via Computational Screening. *ACS Sustainable Chem. Eng.* **2021**, *9*, 8858−8867.
(49) Babaei, H.; McGaughey, A. J. H.; Wilmer, C. E. Effect of pore size and shape on the thermal conductivity of metal-organic frameworks. *Chem. Sci.* **2017**, *8*, 583−589.
(50) Babaei, H.; Wilmer, C. E. Mechanisms of Heat Transfer in Porous Crystals Containing Adsorbed Gases: Applications to Metal-Organic Frameworks. *Phys. Rev. Lett.* **2016**, *116*, 025902.
(51) Han, L.; Budge, M.; Alex Greaney, P. Relationship between thermal conductivity and framework architecture in MOF-5. *Comput. Mater. Sci.* **2014**, *94*, 292−297.
(52) Huang, B. L.; McGaughey, A. J. H.; Kaviany, M. Thermal conductivity of metal-organic framework 5 (MOF-5): Part I. Molecular dynamics simulations. *Int. J. Heat Mass Transfer* **2007**, *50*, 393−404.
(53) Wieme, J.; Vandenbrande, S.; Lamaire, A.; Kapil, V.; Vanduyfhuys, L.; Van Speybroeck, V. Thermal Engineering of Metal−Organic Frameworks for Adsorption Applications: A Molecular Simulation Perspective. *ACS Appl. Mater. Interfaces* **2019**, *11*, 38697−38707.
(54) Babaei, H.; McGaughey, A. J. H.; Wilmer, C. E. Transient Mass and Thermal Transport during Methane Adsorption into the Metal−Organic Framework HKUST-1. *ACS Appl. Mater. Interfaces* **2018**, *10*, 2400−2406.
(55) Babaei, H.; DeCoster, M. E.; Jeong, M.; Hassan, Z. M.; Islamoglu, T.; Baumgart, H.; McGaughey, A. J. H.; Redel, E.; Farha, O. K.; Hopkins, P. E.; et al. Observation of reduced thermal conductivity in a metal-organic framework due to the presence of adsorbates. *Nat. Commun.* **2020**, *11*, 4010.
(56) Klemens, P. In *Thermal Conductivity and Lattice Vibrational Modes*; Seitz, F., Turnbull, D., Eds.; Solid State Physics; Academic Press: 1958; Vol. 7; pp 1 − 98.
(57) Giannozzi, P.; Baroni, S.; Bonini, N.; Calandra, M.; Car, R.; Cavazzoni, C.; Ceresoli, D.; Chiarotti, G. L.; Cococcioni, M.; Dabo, I.; et al. QUANTUM ESPRESSO: a modular and open-source software project for quantum simulations of materials. *J. Phys.: Condens. Matter* **2009**, *21*, 395502.
(58) Giannozzi, P.; Andreussi, O.; Brumme, T.; Bunau, O.; Nardelli, M. B.; Calandra, M.; Car, R.; Cavazzoni, C.; Ceresoli, D.; Cococcioni, M.; et al. Advanced capabilities for materials modelling with Quantum ESPRESSO. *J. Phys.: Condens. Matter* **2017**, *29*, 465901.
(59) Stuart, S. J.; Tutein, A. B.; Harrison, J. A. A reactive potential for hydrocarbons with intermolecular interactions. *J. Chem. Phys.* **2000**, *112*, 6472−6486.
(60) Brenner, D. W.; Shenderova, O. A.; Harrison, J. A.; Stuart, S. J.; Ni, B.; Sinnott, S. B. A second-generation reactive empirical bond order (REBO) potential energy expression for hydrocarbons. *J. Phys.: Condens. Matter* **2002**, *14*, 783.
(61) Giri, A.; Hopkins, P. E. Heat Transfer Mechanisms and Tunable Thermal Conductivity Anisotropy in Two-Dimensional Covalent Organic Frameworks with Adsorbed Gases. *Nano Lett.* **2021**, *21*, 6188−6193.
(62) Rappe, A. K.; Casewit, C. J.; Colwell, K. S.; Goddard, W. A.; Skiff, W. M. UFF, a full periodic table force field for molecular mechanics and molecular dynamics simulations. *J. Am. Chem. Soc.* **1992**, *114*, 10024−10035.
(63) Plimpton, S. Fast parallel algorithms for short-range molecular dynamics. *J. Comput. Phys.* **1995**, *117*, 1−19.
(64) Hoover, W. G. Canonical dynamics: Equilibrium phase-space distributions. *Phys. Rev. A* **1985**, *31*, 1695.
(65) McGaughey, A. J.; Kaviany, M. Quantitative validation of the Boltzmann transport equation phonon thermal conductivity model under the single-mode relaxation time approximation. *Phys. Rev. B* **2004**, *69*, 094303.
(66) Turney, J.; Landry, E.; McGaughey, A.; Amon, C. Predicting phonon properties and thermal conductivity from anharmonic lattice dynamics calculations and molecular dynamics simulations. *Phys. Rev. B* **2009**, *79*, 064301.
(67) Sellan, D. P.; Landry, E. S.; Turney, J.; McGaughey, A. J.; Amon, C. H. Size effects in molecular dynamics thermal conductivity predictions. *Phys. Rev. B* **2010**, *81*, 214305.
(68) Rahman, M. A.; Dionne, C. J.; Giri, A. Pore Size Dictates Anisotropic Thermal Conductivity of Two-Dimensional Covalent Organic Frameworks with Adsorbed Gases. *ACS Appl. Mater. Interfaces* **2022**, *14*, 21687.
(69) Dionne, C. J.; Rahman, M. A.; Hopkins, P. E.; Giri, A. Supramolecular Interactions Lead to Remarkably High Thermal Conductivities in Interpenetrated Two-Dimensional Porous Crystals. *Nano Lett.* **2022**, *22*, 3071−3076.
(70) Thompson, A. P.; Plimpton, S. J.; Mattson, W. General formulation of pressure and stress tensor for arbitrary many-body interaction potentials under periodic boundary conditions. *J. Chem. Phys.* **2009**, *131*, 154107.
(71) Thomas, J. A.; Turney, J. E.; Iutzi, R. M.; Amon, C. H.; McGaughey, A. J. Predicting phonon dispersion relations and lifetimes from the spectral energy density. *Phys. Rev. B* **2010**, *81*, 081411.
(72) Thomas, J. A.; Turney, J. E.; Iutzi, R. M.; Amon, C. H.; McGaughey, A. J. Erratum: Predicting phonon dispersion relations and lifetimes from the spectral energy density [Phys. Rev. B 81, 081411 (R)(2010)]. *Phys. Rev. B* **2015**, *91*, 239905.
(73) Yu, G.; Gao, J.; Hummelen, J. C.; Wudl, F.; Heeger, A. J. Polymer Photovoltaic Cells: Enhanced Efficiencies via a Network of Internal Donor-Acceptor Heterojunctions. *Science* **1995**, *270*, 1789−1791.
(74) Tao, C.; Sun, J.; Zhang, X.; Yamachika, R.; Wegner, D.; Bahri, Y.; Samsonidze, G.; Cohen, M. L.; Louie, S. G.; Tilley, T. D.; et al.


https://doi.org/10.1021/acs.jpcc.3c00652
J. Phys. Chem. C 2023, 127, 11157−11166

Spatial Resolution of a Type II Heterojunction in a Single Bipolar Molecule. *Nano Lett.* **2009**, *9*, 3963−3967.
(75) Casady, J.; Johnson, R. Status of silicon carbide (SiC) as a wide-bandgap semiconductor for high-temperature applications: A review. *Solid-State Electron.* **1996**, *39*, 1409−1422.
(76) Stuart, S. J.; Tutein, A. B.; Harrison, J. A. A reactive potential for hydrocarbons with intermolecular interactions. *J. Chem. Phys.* **2000**, *112*, 6472−6486.
(77) Goodson, K. E. Ordering Up the Minimum Thermal Conductivity of Solids. *Science* **2007**, *315*, 342−343.
(78) Duda, J. C.; Hopkins, P. E.; Shen, Y.; Gupta, M. C. Exceptionally low thermal conductivities of films of the fullerene derivative PCBM. *Phys. Rev. Lett.* **2013**, *110*, 015902.
(79) Thomas, J. A.; Turney, J. E.; Iutzi, R. M.; Amon, C. H.; McGaughey, A. J. H. Predicting phonon dispersion relations and lifetimes from the spectral energy density. *Phys. Rev. B* **2010**, *81*, 081411.





https://doi.org/10.1021/acs.jpcc.3c00652
*J. Phys. Chem. C* 2023, 127, 11157−11166